

LETTERS

Architectural and mechanistic insights into an EHD ATPase involved in membrane remodelling

Oliver Daumke^{1*}†, Richard Lundmark^{1*†}, Yvonne Vallis¹, Sascha Martens¹, P. Jonathan G. Butler¹ & Harvey T. McMahon¹

The ability to actively remodel membranes in response to nucleotide hydrolysis has largely been attributed to GTPases of the dynamin superfamily, and these have been extensively studied¹. Epsin homology (EH)-domain-containing proteins (EHDs/RME-1/pincer) comprise a less-well-characterized class of highly conserved eukaryotic ATPases implicated in clathrin-independent endocytosis², and recycling from endosomes^{3,4}. Here we show that EHDs share many common features with the dynamin superfamily, such as a low affinity for nucleotides, the ability to tubulate liposomes *in vitro*, oligomerization around lipid tubules in ring-like structures and stimulated nucleotide hydrolysis in response to lipid binding. We present the structure of EHD2, bound to a non-hydrolysable ATP analogue, and provide evidence consistent with a role for EHDs in nucleotide-dependent membrane remodelling *in vivo*. The nucleotide-binding domain is involved in dimerization, which creates a highly curved membrane-binding region in the dimer. Oligomerization of dimers occurs on another interface of the nucleotide-binding domain, and this allows us to model the EHD oligomer. We discuss the functional implications of the EHD2 structure for understanding membrane deformation.

EHDs comprise a highly conserved eukaryotic protein family with four members (EHD1–4) in mammals and a single member in *Caenorhabditis elegans*, *Drosophila melanogaster* and in many eukaryotic parasites, such as the genera *Plasmodium*, *Leishmania* and *Entamoeba*. The proteins have a molecular mass of approximately 60 kDa and contain an amino-terminal G-domain, followed by a helical domain and a carboxy-terminal EH-domain (Fig. 1a; in plant homologues the EH-domain is N-terminal). The EH-domain is known to interact with Asn-Pro-Phe (NPF) motifs in proteins involved in endocytosis. Overexpressed EHDs can be found on tubules inside cells and EHD family members (including RME-1/EHD1 and pincer) have been shown to regulate exit from the endocytic recycling compartment, TrkA-receptor-mediated macro-pinocytosis and other trafficking pathways^{2–12}. Here we explore the structure and function of mouse EHD2 as a model for the EHD family.

Mouse full-length EHD2 was expressed in bacteria and purified to homogeneity (Supplementary Fig. 1). The purified protein was nucleotide-free, as judged by HPLC analysis, and was dimeric in analytical velocity centrifugation (Supplementary Fig. 2). It was previously reported that EHDs—despite having a predicted G-domain—bind to adenine nucleotides¹³. We confirmed these results by using isothermal titration calorimetry: the affinities for ATP- γ -S and ADP were 13 μ M and 50 μ M, respectively (Fig. 1b). Nucleotide binding was Mg^{2+} -dependent (data not shown). A mutation in the GKT motif in the phosphate-binding (P-)loop, T72A, prevented binding

to ATP- γ -S in a manner similar to that of equivalent mutations in other GTPases. No binding signal was observed for GTP- γ -S (Fig. 1b). We still refer to the N-terminal domain as a G-domain because of sequence and fold similarity (see below) to other G-domains. We investigated membrane-binding properties of EHD2 and found efficient binding to liposomes of brain-derived lipids (Folch extract) and to 100% anionic phosphatidyl-serine (PtdSer) liposomes (Fig. 1c). However, using synthetic liposomes containing different phosphatidyl inositol (PtdIns) and more stringent conditions (only 10% PtdSer, Fig. 1c), we observed preferential binding to liposomes containing PtdIns(4,5)bisphosphate, PtdIns(4,5)P₂.

The consequence of membrane binding was analysed by electron microscopy, and we found that EHD2 deforms PtdSer liposomes in a nucleotide-independent manner into 20-nm diameter tubules and oligomerizes in ring-like structures around these tubules (Fig. 1d, and Supplementary Fig. 3). Nucleotide independence of liposome tubulation *in vitro* was also observed for dynamin¹. No noticeable tubule fission or alteration in tubule diameter was found for EHD2 in the presence of ATP. Frequently, we observed a complex network of connected tubules that had an extensive surface area, implying that there is considerable fusion occurring between liposomes (Supplementary Fig. 3). We also saw a few instances where EHD2 oligomeric rings were of variable diameter (Fig. 1d, right panel) suggesting that the interface used for EHD2 oligomerization is rather flexible. Folch liposomes were also tubulated by EHD2 in a nucleotide-independent manner (data not shown). However, with synthetic liposomes containing only 2.5% PtdIns(4,5)P₂ and in the absence of PtdSer, the amount of EHD binding was reduced, and in this less-favourable binding condition we only observed tubulation in the presence of ATP- γ -S and ADP, but not in the absence of nucleotides (Supplementary Fig. 3).

When enhanced green fluorescent protein (EGFP)-tagged EHD2 was overexpressed in HeLa cells it marked punctate and tubular structures (Fig. 1e, endogenous EHD2 in various cell lines shows a similar peripheral distribution^{5,14}). By total internal reflection fluorescence microscopy, those structures were mainly found close to the plasma membrane (data not shown), consistent with the observed PtdIns(4,5)P₂ specificity. Although the nucleotide-free T72A mutant bound to Folch liposomes *in vitro* (Fig. 1c), it showed a cytoplasmic distribution when overexpressed *in vivo* (Fig. 1e), indicating that nucleotide binding is required for oligomerization *in vivo*, in agreement with previous results³.

The effect of membrane binding on the ATPase activity of EHD2 was monitored under multiple-turnover conditions (tenfold excess of ATP over EHD2), in the presence and absence of Folch liposomes (Fig. 1f, and Supplementary Fig. 4). The intrinsic/background

¹MRC Laboratory of Molecular Biology, Hills Road, Cambridge, CB2 0QH, UK. [†]Present addresses: Max-Delbrück-Centrum für Molekulare Medizin (MDC), Robert-Rössle-Str. 10, 13092 Berlin, Germany (O.D.); Umeå University, Department of Medical Biochemistry and Biophysics, 90187 Umeå, Sweden (R.L.).

*These authors contributed equally to this work.

ATPase activity is extremely slow ($k_{\text{obs}} = 0.7 \text{ h}^{-1}$) but is stimulated by liposome binding and can be maximally activated eightfold in the presence of saturating Folch or PtdSer liposomes ($k_{\text{obs}} = 5.6 \text{ h}^{-1}$). In contrast to GBP1 (ref. 15), we did not observe hydrolysis to nucleoside mono-phosphate. GTP was not hydrolysed in the presence or absence of Folch liposomes, and the T72A mutant did not show membrane-stimulated ATPase activity. EHD2 displays a 600-fold slower stimulated nucleotide hydrolysis than dynamin, which hydrolyses GTP under our standard conditions (see Methods) with a k_{cat} of $\approx 1 \text{ s}^{-1}$.

To obtain structural insights, we solved the crystal structure of EHD2 in the presence of the non-hydrolysable ATP analogue AMP-PNP (see Methods, Table 1 and Supplementary Table 1 for the statistics). The nucleotide-binding domain of EHD2 possesses a typical G-domain fold with a central β -sheet surrounded by α -helices (Fig. 2a, b, and Supplementary Fig. 5). An AMP-PNP molecule occupies the canonical nucleotide-binding site. In comparison to the Ras-like G-domain, EHD2 contains an insertion of two additional β -strands in the switch I region, which are also present in the G-domain of dynamin¹⁶ (Fig. 2b). Surprisingly, switch I and switch II are not well ordered in this dimeric protein (Fig. 2a). Residues 110–130, which are distal to switch I, are disordered and contain predicted EH-domain binding motifs, KPFxxxNPF. In agreement with our biochemical analysis, EHD2 crystallizes as a dimer, and the dimer axis corresponds to a crystallographic two-fold axis (Fig. 2a). Dimerization is mediated by a highly conserved, mostly hydrophobic interface of approximately $2,100 \text{ \AA}^2$ in the G-domain (Supplementary Fig. 6). At the centre of the interface, the entirely conserved W238 in helix α 6 is buried in a hydrophobic pocket, and mutations of this residue render the protein insoluble (data not shown). This novel interface is highly conserved among EHD family members and involves a different face of the G-domain to the dimer

Table 1 | X-ray refinement statistics

Resolution (Å)	20–3.1
Number of reflections	12,091
$R_{\text{work}}/R_{\text{free}} (\%)$	23.6/27.6
Number of atoms	
Protein	3,765
Ligand/ion	33
Water	6
B-factors	
Protein	61 \AA^2
Ligand/ion	50 \AA^2
Water	51.5 \AA^2
Root mean squared deviations	
Bond lengths (Å)	0.019
Bond angles (°)	1.119

interfaces from the structurally characterized GBP1 and bacterial dynamin-like protein (BDLP) dimers^{15,17}.

The helical domain is composed of helix α 1 and α 2 from the N-terminal region (residues 18–55, which follow disordered residues 1–18) and helices α 8 to α 12 (residues 285–400) following the G-domain (Fig. 2a,b). Helix α 8 is the organizing scaffold against which most of the other helices fold. It also has extensive contacts with the G-domain. The dimeric G-domain, together with the helical region, adopts a scissor shape, in which the membrane is proposed to bind between the blades (see later). Following the middle domain, a 40-residue linker connects the helical domain with the C-terminal EH-domain (residues 443–543). The EH-domain of EHD2 is similar to the previously determined second EH-domain of Eps15 solved by NMR studies^{18,19}, with a root mean squared deviation of 1.5 \AA for the main-chain atoms (Fig. 2c). It is built of two closely packed perpendicular EF hands, which are connected by a short β -sheet. We included a Ca^{2+} -ion in the second EF hand, which is ligated by four oxygens from acidic side chains and one main-chain carbonyl oxygen

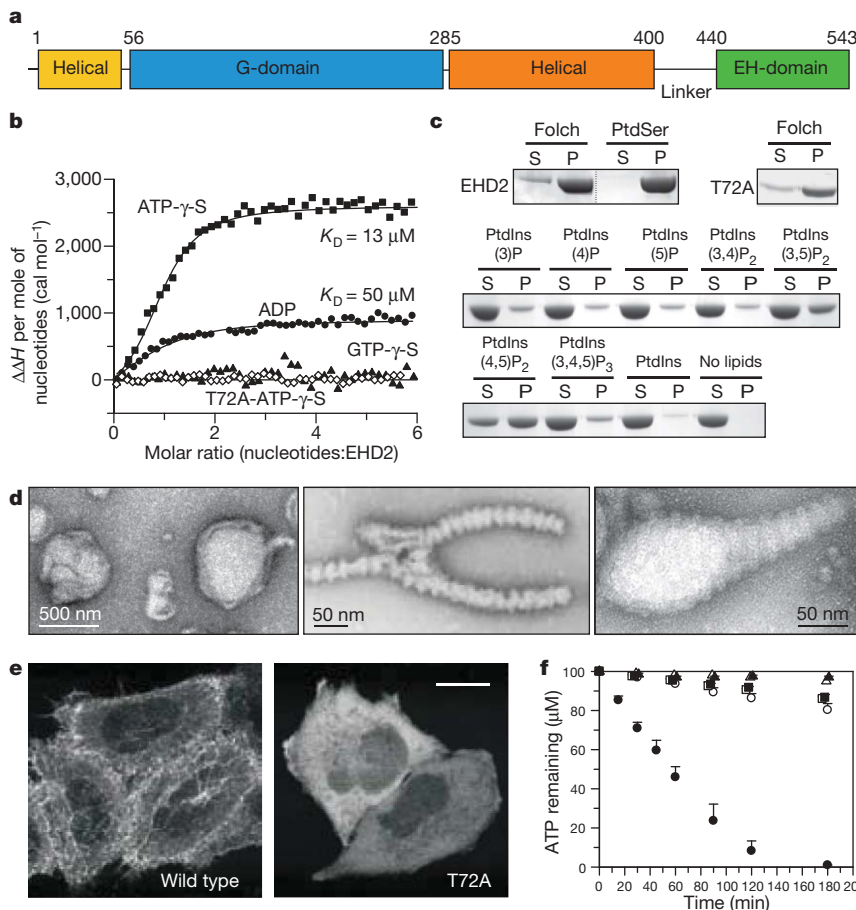


Figure 1 | EHD2 shares common properties with the dynamin superfamily. **a**, Domain structure of EHD proteins (numbering from mouse EHD2 amino acids). **b**, EHD2 binds to adenine nucleotides, as determined by isothermal titration calorimetry. For clarity, $\Delta\Delta H = \Delta H_n - \Delta H_1$ is plotted. **c**, Coomassie-stained gels of liposome co-sedimentation assays in the presence of 1 mM ATP- γ -S using 0.8- μm -filtered Folch, 100% PtdSer or synthetic liposomes containing 10% of the indicated PtdIns (plus 70% Ptd choline, 10% PtdSer, 10% cholesterol). S, supernatant; P, pelleted fraction. **d**, Electron micrographs of negatively stained PtdSer liposomes in the absence (left panel) or presence (middle, right panels) of EHD2 and 1 mM ATP- γ -S. The right panel shows an intermediate in the tubulation process, surrounded by EHD2 rings of variable diameter. **e**, Amino-terminally EGFP-tagged EHD2 wild type and the T72A mutant were overexpressed in HeLa cells. Confocal images were acquired close to the basal cell surface; the scale bar is 10 μm . **f**, Nucleotide hydrolysis by EHD2 was measured by HPLC. Intrinsic reactions in absence of lipids are open symbols (mean \pm s.d., $n = 2$) and stimulated reactions are filled symbols (mean \pm s.d., $n = 3$). Whereas the intrinsic ATP reaction was eightfold-stimulated by Folch lipids (open versus filled circles), GTP hydrolysis was not stimulated (open versus filled triangles). The nucleotide-free T72A mutant did not show stimulation of ATP hydrolysis (open versus filled squares).

(Supplementary Fig. 7a). The EH-domain is localized on top of the G-domain (the top-site position) with a buried interface of 1,600 Å². Eighteen disordered residues connecting the EH-domain to the helical domain mean that it is ambiguous which EH-domain connects to which helical domain. We assign the EH-domains to opposing monomers (red EH-domain belongs to the red helical domain in Fig. 2a) because the last visible residue of the linker from the helical domain is closer to the opposite EH-domain (distance 29 Å) than to the superjacent EH-domain (distance of 34 Å), and, in this latter case, the linker would have to wind around the EH-domain and thus one would expect to see some parts of this in the structure (Fig. 2a). Unexpectedly, the peptide-binding sites of both EH-domains are occupied by a GPF motif (residues 420–422) from the linker region (Fig. 2a and c). The GPF motif adopts a similar conformation to an NPF-containing peptide bound to the EH2 domain of Eps15 (ref. 18), involving a tight turn with F422 projecting into a hydrophobic pocket that is lined by W490 at its base (Fig. 2c and Supplementary Fig. 7a). R536 in the C-terminal tail of the EH-domain points into the active site of the G-domain below and forms a hydrogen bond to D222 from the NKxD motif, which in other GTPases is responsible for specific recognition of the guanosine base (see Supplementary Fig. 8 for details). Furthermore, M223 sterically prevents binding of GTP, thus explaining the ATP specificity of EHD2.

To test if a polybasic stretch close to the tip of the helical domain was involved in lipid binding, we monitored lipid binding of K327D, K328D and also F322A (Fig. 3a). These mutants showed reduced liposome binding and ATPase activity in the presence of Folch liposomes (Fig. 3b, c). *In vivo*, F322A, and every lysine to aspartate mutation of K324, K327, K328, K329, led to a cytoplasmic distribution of the protein (Fig. 3d, and data not shown). Thus, the lipid interaction site of EHD2 is composed of two closely apposing lipid-binding sites in the dimer, leading to a highly curved membrane-binding interface (Fig. 3a, and Supplementary Fig. 9). Under stringent binding conditions, EHD2 indeed showed a binding preference for very small liposomes, consistent with this curvature, but only in the nucleotide-free form (Supplementary Fig. 9). In the nucleotide-bound form, EHD2 binding was not curvature-sensitive, and this is probably due to oligomer formation along an axis perpendicular to the high curvature (see below).

In EHD2, the phosphate groups of the AMP-PNP molecule are occluded from the exterior by a 'phosphate cap' that is formed by

switch I and the P-loop, which would not allow the insertion of a catalytic residue *in trans* into the catalytic site (Supplementary Fig. 10). We searched for *in cis* catalytic residues and found that the switch I mutant T94A bound to ATP-γ-S with nearly wild-type affinity and oligomerized around PtdSer liposomes, but did not show any membrane-stimulated ATPase activity (Fig. 3e). This is consistent with a catalytic function for T94. When overexpressed in HeLa cells, the T94A mutant labelled extensive tubular structures with essentially no punctate staining (compare wild type and T94A in Fig. 3d, f and g, and Supplementary Movies 1–4), suggesting that ATP hydrolysis is involved in the break-down of tubular structures *in vivo*. We previously observed severely inhibited GTP hydrolysis and an extensive tubulation phenotype (like that found with EHD2 T94A) with dynamin 1 when T65 in switch I was mutated to alanine²⁰. We analysed another mutant in switch II, in which a glutamine was introduced close to the catalytic site. I157Q hydrolysed ATP faster than wild type, even in the absence of membranes and tubulated liposomes (Fig. 3e). When overexpressed in HeLa cells this protein labelled only very short tubules and puncta (Fig. 3f, g). Many of these puncta were highly mobile as determined by live-cell microscopy (Supplementary Movies 5, 6). Thus, there is a clear correlation between the measured ATP hydrolysis rates *in vitro* and the extent of tubule formation *in vivo*. The ATPase rates might be further stimulated *in vivo*, by binding partners or modifications. Altogether, these results are consistent with a role of EHD2 ATP hydrolysis in membrane remodelling and/or the scission of membranes *in vivo*.

A highly conserved surface patch encompasses switch I, switch II and the surrounding area of the EHD2 dimer (Fig. 4a). GBP1 and BDLP use this same interface, with the same relative orientation of the G-domains, for dimerization^{15,17}. Thus, the EHD2 dimer may further oligomerize into the observed rings (Fig. 1d) using this second G-domain interface. This oligomerization probably leads to the ordering of residues in the switch regions, leading to increased nucleotide hydrolysis. Four single mutations of conserved surface-exposed residues in this interface did not affect lipid binding or oligomerization on liposomes but greatly reduced the liposome-stimulated ATPase reaction (Fig. 4b, Supplementary Fig. 11a). The most drastic mutant, K193D, was further tested *in vivo* and showed extensive tubulation, whereas the E91Q mutant, which had the mildest effect on the stimulated ATPase reaction, was indistinguishable from wild type *in vivo* (Supplementary Fig. 11b). These results are

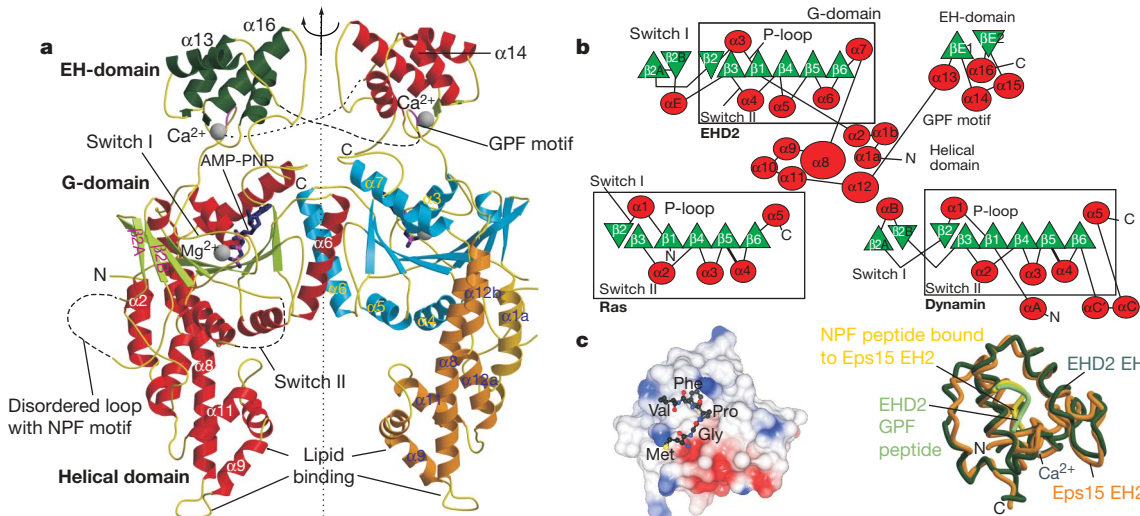


Figure 2 | The structure of EHD2. **a**, Ribbon-type presentation of the EHD2 dimer (PDB code 2QPT). One molecule is coloured according to the secondary structure (helices in red, β-strands in green) and the other according to the domain structure (see Fig. 1a). GPF and NPF motifs are indicated. **b**, Topology plot of EHD2 (circles represent α-helices, triangles represent β-strands). EHD2 has a dynamin-related switch I extension when

compared with the classical Ras-like G-domain (boxed) and the dynamin G-domain. **c**, Left panel, electrostatic surface representation of the EHD2 EH-domain (at neutral pH: red, negative; blue, positive). F422 is penetrating in the non-charged peptide-binding pocket. Right panel, close superposition of the EHD2 EH-domain (dark-green) with the second EH-domain of Eps15 (orange) bound to an NPF-containing peptide (PDB code 1FF1)¹⁹.

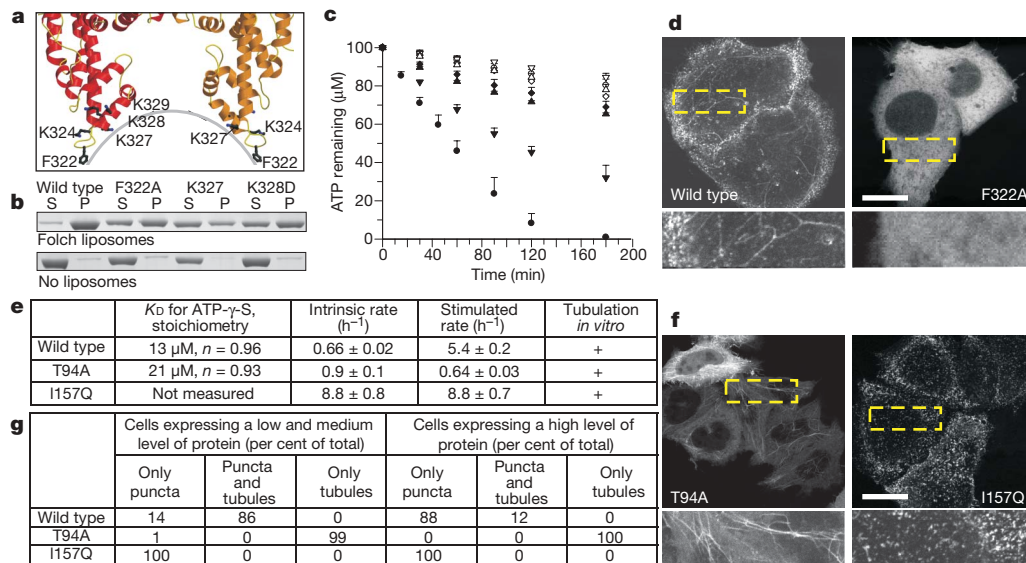


Figure 3 | Membrane binding and the role of ATP hydrolysis. **a**, Putative membrane-binding site with residues tested for membrane binding in ball-and-stick representation. The highly curved membrane interaction site of EHD2 is indicated. **b**, Sedimentation assays in the presence (upper panel) and absence (lower panel) of Folch liposomes using wild-type EHD2 and mutants, as in Fig. 1c. **c**, Nucleotide hydrolysis of lipid binding mutants as described in Fig. 1f. The wild-type protein had a k_{obs} of 1.6 h^{-1} (open circles, intrinsic; filled circles, lipid stimulated). The F322A mutant (open versus filled inverted triangles) showed a 40% decrease in the stimulated ATPase reaction ($k_{obs} = 3.0 \text{ h}^{-1}$), and the K328D mutant (open versus filled triangles) showed a 75% reduced rate ($k_{obs} = 1.6 \text{ h}^{-1}$), whereas for the

K327D mutant (open versus filled diamonds) stimulation was barely visible. **d**, EGFP-tagged F322A mutant showed a completely cytoplasmic distribution when overexpressed in HeLa cells. Scale bar, $10 \mu\text{m}$. **e**, Affinity to ATP- γ -S was measured as in Fig. 1b. Nucleotide hydrolysis was measured as described in Fig. 1f (values represent mean \pm s.e.m.; n = 2, intrinsic; n = 3, stimulated reactions). *In vitro* tubulation activity of PtdSer liposomes was analysed as described in Fig. 1d. **f**, Confocal images of HeLa cells overexpressing the indicated mutants. Scale bar, $10 \mu\text{m}$. **g**, Quantification of the overexpression phenotypes from Fig. 3f. For each construct, three independent experiments with ≈ 50 cells per experiment were analysed.

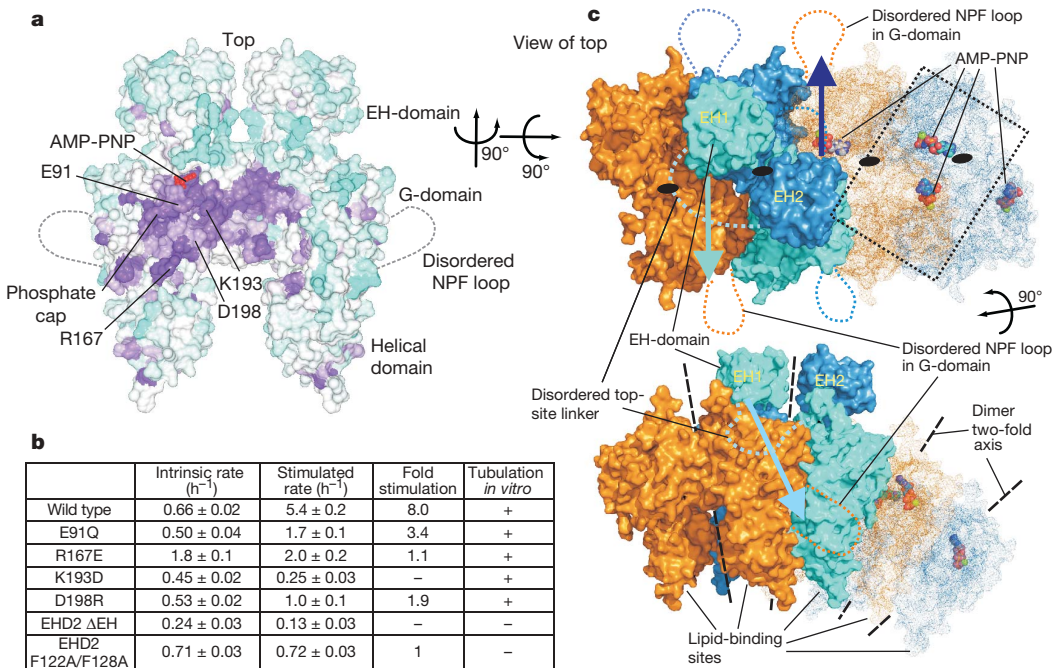


Figure 4 | The EHD2 oligomer. **a**, Surface conservation plot of the EHD2 dimer (in the same orientation as in Fig. 2a, using the alignment in Supplementary Fig. 5) with conserved residues in purple and non-conserved residues in cyan. Conserved surface-exposed residues mutated in the following experiments are indicated. The relative orientation of the dimers in Fig. 4c is also indicated by arrows. **b**, Nucleotide hydrolysis (as in Fig. 1f) for mutants in the proposed oligomerization interface. Note that mutant R167E (in switch II) showed an increased basal ATPase activity, which was not further stimulated by Folch liposomes. Tubulation of PtdSer liposomes was assayed by negative-stain electron microscopy as in Fig. 1d. **c**, Model of the EHD2 oligomer. Upper

panel, top view of the proposed oligomer, limited to four EHD2 dimers, in which the two-fold axis of the dimers is indicated by the black oval. Only the blue-cyan dimer has its EH-domains included so that the proposed movement of the EH-domains from the top-site linker to the side-site of the G-domain can be better visualized (see arrows for movements). The AMP-PNP molecules face each other in a head-to-head fashion diagonally across each dimer interface (see dotted box), as seen in the GBP1 and BDLP dimers. Lower panel, sideward view of the proposed oligomer; the membrane-binding sites are facing all in the same direction towards the putative membrane interface. Movies are available at <http://www.endocytosis.org/EHDs/>.

consistent with this interface being involved in oligomerization-dependent reorientation of residues responsible for ATP hydrolysis. Using the dimeric GBP1•GDP•AlF₃ G-domain structure¹⁵ as a template and taking into account the observed 20-nm ring of the EHD2 coat (Fig. 1d), we predicted the arrangement of the EHD2 dimers within the oligomer, in which the nucleotides of two opposing EHD monomers are facing each other in a head-to-head fashion (see Methods and Fig. 4c). The predicted oligomer has a compact structure with a high degree of shape-complementarity between the oligomerizing dimers (Supplementary coordinates). Furthermore, the membrane-binding sites are pointing in the same direction towards the putative membrane interface (Fig. 4c, Supplementary Fig. 12a), and the thickness of the oligomeric ring agrees well with the thickness of the rings observed by electron microscopy (≈ 10 nm, Fig. 1d). In the predicted oligomer, the highly curved membrane interface of the EHD2 dimer is oriented perpendicular to the direction of the tubule curvature (Supplementary Fig. 12b, c). Furthermore, the disordered surface loop at the side of the G-domain containing the two conserved PF motifs (NPF and KPF) comes into the vicinity of the EH-domain linker (Fig. 4c and Supplementary Fig. 7b). Thus, we speculated that the EH-domain might switch position from the observed top site in the dimer in solution to the side-site position of the opposing dimer, during oligomerization (Fig. 4c). Interestingly, only a side-site NPF peptide, and not the top-site GPF peptide, bound with a measurable affinity (≈ 130 μ M) to the isolated EH-domain of EHD2 (Supplementary Fig. 7c). Furthermore, in agreement with our prediction we observed that a deletion mutant of the EH-domain (Δ EH) or a double mutant of the two side-site xPF motifs (F122A/F128A) did not show any membrane-stimulated ATPase activity (Fig. 4b), and we did not find any regular oligomers on liposomes in electron microscopy studies for these mutants (see Supplementary Fig. 7 for further discussion).

On the basis of the conservation of structural and mechanistic elements we propose to expand the dynamin superfamily to include other multidomain large G-domain proteins such as EHDs and BDLPs. The structure outlined above, the architecture of the membrane interaction site and the proposed oligomer provide a framework to understand membrane remodelling for the EHD family, and perhaps for dynamin superfamily members. The EHD2 dimer interacts with membranes via ionic interactions mediated by a highly curved interface and we predict that this interaction results in the insertions of V321 and F322 into the hydrophobic phase of the lipid bilayer. Both the curved interface and the hydrophobic residue insertions (see synaptotagmin²¹) will result in the bending of the membrane towards the EHD2 dimer (buckling). The membrane curvature imposed by our proposed oligomer would be perpendicular to the curvature imposed by the concave membrane-binding face of the EHD2 dimer (Supplementary Fig. 12b). This would cause considerable curvature stress in the lipid bilayer and would thus facilitate the lipid rearrangement required for the formation of intermediate stages towards membrane fission/fusion²². Finally we observe that nucleotide hydrolysis is most probably leading to membrane scission *in vivo*, and thus we would argue that conformational changes induced by nucleotide hydrolysis are transmitted through helix 8 to the membrane-binding interface leading to further membrane destabilization.

METHODS SUMMARY

Isothermal titration calorimetry measurements were performed at 10 °C in 20 mM HEPES (pH 7.5), 300 mM NaCl, 2 mM MgCl₂. Liposome binding assays were performed using 0.33 mg ml⁻¹ of 0.8- μ m-filtered liposomes as described previously (www.endocytosis.org). For electron microscopic studies, 2.5 μ M EHD2 in 20 mM HEPES (pH 7.5), 150 mM NaCl, 1 mM MgCl₂ was incubated for 15 min at 25 °C in the presence of 1 mM nucleotide and 0.05 mg ml⁻¹ (final

concentration) of the indicated 0.8- μ m-filtered liposomes. Samples were spotted on carbon-coated copper grids (Canemco and Marivac) and negatively stained with 2% uranyl acetate.

Full Methods and any associated references are available in the online version of the paper at www.nature.com/nature.

Received 21 June; accepted 15 August 2007.

Published online 3 October 2007.

- Praefcke, G. J. & McMahon, H. T. The dynamin superfamily: universal membrane tubulation and fission molecules? *Nature Rev. Mol. Cell Biol.* **5**, 133–147 (2004).
- Shao, Y. et al. Pincher, a pinocytic chaperone for nerve growth factor/TrkA signaling endosomes. *J. Cell Biol.* **157**, 679–691 (2002).
- Grant, B. et al. Evidence that RME-1, a conserved *C. elegans* EH-domain protein, functions in endocytic recycling. *Nature Cell Biol.* **3**, 573–579 (2001).
- Caplan, S. et al. A tubular EHD1-containing compartment involved in the recycling of major histocompatibility complex class I molecules to the plasma membrane. *EMBO J.* **21**, 2557–2567 (2002).
- Blume, J. J., Halbach, A., Behrendt, D., Paulsson, M. & Plomann, M. EHD proteins are associated with tubular and vesicular compartments and interact with specific phospholipids. *Exp. Cell Res.* **313**, 219–231 (2007).
- George, M. et al. Shared as well as distinct roles of EHD proteins revealed by biochemical and functional comparisons in mammalian cells and *C. elegans*. *BMC Cell Biol.* **8**, 3 (2007).
- Jovic, M., Naslavsky, N., Rapaport, D., Horowitz, M. & Caplan, S. EHD1 regulates β 1 integrin endosomal transport: effects on focal adhesions, cell spreading and migration. *J. Cell Sci.* **120**, 802–814 (2007).
- Lin, S. X., Grant, B., Hirsh, D. & Maxfield, F. R. Rme-1 regulates the distribution and function of the endocytic recycling compartment in mammalian cells. *Nature Cell Biol.* **3**, 567–572 (2001).
- Park, S. Y. et al. EHD2 interacts with the insulin-responsive glucose transporter (GLUT4) in rat adipocytes and may participate in insulin-induced GLUT4 recruitment. *Biochemistry* **43**, 7552–7562 (2004).
- Rotem-Yehudar, R., Galperin, E. & Horowitz, M. Association of insulin-like growth factor 1 receptor with EHD1 and SNAP29. *J. Biol. Chem.* **276**, 33054–33060 (2001).
- Valdez, G. et al. Pincher-mediated macroendocytosis underlies retrograde signaling by neurotrophin receptors. *J. Neurosci.* **25**, 5236–5247 (2005).
- Braun, A. et al. EHD proteins associate with syndapin I and II and such interactions play a crucial role in endosomal recycling. *Mol. Biol. Cell* **16**, 3642–3658 (2005).
- Lee, D. W. et al. ATP binding regulates oligomerization and endosome association of RME-1 family proteins. *J. Biol. Chem.* **280**, 17213–17220 (2005).
- Guilherme, A. et al. EHD2 and the novel EH domain binding protein EHBPI couple endocytosis to the actin cytoskeleton. *J. Biol. Chem.* **279**, 10593–10605 (2004).
- Ghosh, A., Praefcke, G. J., Renault, L., Wittinghofer, A. & Herrmann, C. How guanylate-binding proteins achieve assembly-stimulated processive cleavage of GTP to GMP. *Nature* **440**, 101–104 (2006).
- Reubold, T. F. et al. Crystal structure of the GTPase domain of rat dynamin 1. *Proc. Natl. Acad. Sci. USA* **102**, 13093–13098 (2005).
- Low, H. H. & Lowe, J. A bacterial dynamin-like protein. *Nature* **444**, 766–769 (2006).
- de Beer, T., Carter, R. E., Lobel-Rice, K. E., Sorkin, A. & Overduin, M. Structure and Asn-Pro-Phe binding pocket of the Eps15 homology domain. *Science* **281**, 1357–1360 (1998).
- de Beer, T. et al. Molecular mechanism of NPF recognition by EH domains. *Nature Struct. Biol.* **7**, 1018–1022 (2000).
- Marks, B. et al. GTPase activity of dynamin and resulting conformation change are essential for endocytosis. *Nature* **410**, 231–235 (2001).
- Martens, S., Kozlov, M. M. & McMahon, H. T. How synaptotagmin promotes membrane fusion. *Science* **316**, 1205–1208 (2007).
- Zimmerberg, J. & Kozlov, M. M. How proteins produce cellular membrane curvature. *Nature Rev. Mol. Cell Biol.* **7**, 9–19 (2006).

Supplementary Information is linked to the online version of the paper at www.nature.com/nature.

Acknowledgements Long-term fellowships supported O.D. (The International Human Frontier Science Program Organization), R.L. (Swedish Research Council) and S.M. (EMBO). We thank M. Plomann for providing the complementary DNAs for mammalian EHDs, and the ESRF beam staff in Grenoble for their support. The authors declare no competing financial interests.

Author Information The atomic coordinates of mouse EHD2 have been deposited in the Protein Data Bank (PDB) with the accession number 2QPT. Reprints and permissions information is available at www.nature.com/reprints. The authors declare no competing financial interests. Correspondence and requests for materials should be addressed to H.T.McM. (hmm@mrc-lmb.cam.ac.uk) or O.D. (oliver.daumke@mdc-berlin.de).

METHODS

Protein expression and structure determination. Mouse EHD2 full-length protein, the Δ EH-domain construct (amino acids 1–404) and all mutants were expressed as N-terminal His-fusions followed by a PreScission cleavage site in *Escherichia coli* BL21 DE3 Rosetta (Novagen) from a modified pET28 vector. Bacterial cultures in TB medium were induced at a OD_{600} of 0.2 with 40 μ M IPTG, and grown overnight at 18 °C. Bacteria were lysed in 50 mM HEPES (pH 7.5), 400 mM NaCl, 25 mM imidazole, 2.5 mM β -mercaptoethanol, 500 μ M Pefablock SC (Boehringer Ingelheim) using an Emulsiflex homogenizer (Avestin). After centrifugation at 100,000g for 45 min at 4 °C, the soluble extract was applied to a NiNTA-column (Qiagen) equilibrated with lysis buffer. The column was extensively washed with 20 mM HEPES (pH 7.5), 700 mM NaCl, 30 mM imidazole, 2.5 mM β -mercaptoethanol, 1 mM ATP, 10 mM KCl, and shortly with 20 mM HEPES (pH 7.5), 300 mM NaCl, 25 mM imidazole, 2.5 mM β -mercaptoethanol. Bound protein was eluted with 20 mM HEPES (pH 7.5), 300 mM NaCl, 100 mM imidazole, 2.5 mM β -mercaptoethanol, and dialysed overnight at 4 °C against 20 mM HEPES (pH 7.5), 300 mM NaCl, 2.5 mM β -mercaptoethanol in the presence of 250 μ g PreScission protease to cleave the His-tag. The protein was re-applied to a NiNTA column to which it bound under these buffer conditions in the absence of the His-tag. The column was extensively washed with 20 mM HEPES, 300 mM NaCl, 2.5 mM β -mercaptoethanol, and the protein finally eluted with 20 mM HEPES, 300 mM NaCl, 2.5 mM β -mercaptoethanol, 25 mM imidazole, concentrated and further purified using a Sephadex200 size-exclusion column (two consecutive runs for proteins used for the ATPase assays). Typical yields were 4 mg of purified EHD2/1 bacterial culture. At 300 mM NaCl, we could concentrate the protein to 40 mg ml⁻¹, but at lower salt concentration we observed some precipitation at this protein concentration. The protein was partially stabilized by 1 mM MgCl₂.

ATPase assays. Multiple turnover ATPase assays were performed in 20 mM HEPES (pH 7.5), 135 mM NaCl, 15 mM KCl, 1 mM MgCl₂ at 30 °C with 10 μ M EHD2 (or mutants) as enzyme and 100 μ M ATP as substrate, in the absence or presence of 1 mg ml⁻¹ sonicated Folch (Sigma-Aldrich) liposomes, with an average diameter of 135 nm, as determined by dynamic light scattering. Reactions were started by the addition of the protein to the final reaction mix and nucleotide hydrolysis was followed using standard HPLC measurement²³. Initial rates were determined by applying a linear fit to data points up to 40% nucleotide hydrolysis. For the dynamin reaction, 1 μ M of protein with 1 mM of GTP as substrate has been used.

Crystallization and structure determination. For crystallization, a selenomethionine-substituted point mutant Q410A was prepared, as described²⁴. This mutant showed identical biochemical properties as the wild-type protein but displayed less degradation in the linker region when incubated over longer periods of time. The protein was concentrated to 40 mg ml⁻¹ and supplemented with 4 mM MgCl₂, 2 mM AMP-PNP (Sigma-Aldrich; both final concentrations). The hanging-drop vapour-diffusion method was used for crystallization. Protein solution (2 μ l) was mixed with an equal volume of reservoir solution containing 3% PEG2000 MME, 50 mM MES (pH 6.4), 4 mM MgCl₂. Crystals appeared after one week at 4 °C and had dimensions of \approx 0.2 \times 0.2 \times 0.05 mm³. For flash-freezing in liquid nitrogen, they were first transferred for 10 s into 50 mM MES (pH 6.4), 75 mM NaCl, 4 mM MgCl₂, 2 mM AMP-PNP, 14% MPD before incubation in the final cryo-solution containing 50 mM MES (pH 6.4), 75 mM NaCl, 4 mM MgCl₂, 2 mM AMP-PNP, 27% MPD. No crystals were obtained in the presence of ADP or in nucleotide-free conditions.

One data set at the selenium peak wavelength was collected from a single crystal at the ESRF beamline ID14-EH4 (see Supplementary Table 1) and processed and scaled using the Xds program suite²⁵. Crystals belonged to the monoclinic crystal system and contained one molecule in the asymmetric unit. Thirteen out of sixteen selenium atoms were found from SHELXD²⁶ using the anomalous signal of the data set. Selenium sites were refined and initial phases were calculated using the program SHARP²⁷. In the resulting electron density, the main chain was clearly traceable, and an initial model could be built using the XtalView package²⁸. The model was refined using Refmac5 (ref. 29) with 3 TLS groups (Table 1). The asymmetric unit contains 477 amino acids, one AMP-PNP, one magnesium, one calcium and five water molecules and has an excellent geometry with all residues in the favoured and most favoured region of the Ramachandran plot as judged by the program Procheck³⁰. Ribbon plots were prepared using the program Molscript³¹ and rendered with Raster3D³². Surface conservation plots were prepared using the ConSurf server³³ and Ccp4 molecular graphics³⁴. Electron potential maps were generated using Ccp4 molecular graphics. All other surface representations were prepared using Pymol³⁵. To predict the arrangement of the EHD2 dimer in the oligomer, two EHD2 dimers were superimposed with one of the two monomers of the GBP1•GDP•AlF₃-dimer (PDB

code 2B92) using SwissPdb viewer³⁶. The EHD2 dimers were manually realigned to avoid amino acid clashes such that the two-fold axis between the oligomerizing EHD2 monomers was maintained. A high degree of shape complementarity between the EHD2 dimers in the resulting tetramer supported this approach (Supplementary Fig. 11). Furthermore, the lipid-binding sites of both EHD2 dimers are expected to contact the membrane, and this restraint is fulfilled in the tetramer. To obtain a 20 nm ring, an 18° tilt was introduced between the dimers. We refrained from energy-minimising of this structure because major conformational changes in the interface are expected to take place on oligomerization (ordering of switch I and switch II) and the resolution of the structure is not appropriate for an accurate prediction. The programs Superpose and Pdbset from Ccp4 (ref. 37) were used to generate the oligomer from the tetramer. PDB coordinates of the proposed oligomer are found in the Supplementary Materials. Additional movies of the EHD structure will be posted on <http://www.endocytosis.org/EHDS/>.

Ultracentrifugation. Sedimentation velocity experiments were performed in a Beckman Optima XLA ultracentrifuge, using an An-60Ti rotor. Centrifugation was at 50,000 revolutions min⁻¹ and 5 °C at an EHD2 concentration of 15 μ M, with scans as fast as possible (\sim 1.5 min intervals). The data were analysed using DCDT+ v.2 (refs 38, 39), with the partial specific volume for the protein (from the amino acid composition) and solvent density and viscosity calculated using Sednterp⁴⁰. Selected scans (at equal, \sim 15 min intervals), of $g(s_{20,w})$ (the amount of material sedimenting between $s_{20,w}$ and $s_{20,w} + \delta s$) and also the residuals for fitting the data with DCDT+, were plotted with the program Profit v.5.6.7 (Quantum soft).

Cell biology. Amino-terminal EGFP-tagged EHD2 and all mutants were over-expressed in HeLa cells from the pEGFP-C3 vector (Clontech). HeLa cells were grown in DMEM containing 10% fetal bovine serum and transfected using Genejuice (Novagen) for transient protein expression. Twenty four hours after transfection, cells were fixed for 20 min at 37 °C in 3.2% paraformaldehyde and mounted. All confocal images were taken sequentially using a BioRad Radiance system and LaserSharp software (Biorad). For real-time microscopy, transfected cells on glass-bottom Petri dishes (WillCo Wells BV) were washed with 25 mM HEPES (pH 7.5), 125 mM NaCl, 5 mM KCl, 10 mM D-glucose, 1 mM MgCl₂, 2 mM CaCl₂, and epifluorescence images were taken using an Olympus IX70 microscope (Southhall) and Argon laser (Melles Griot) with a Princeton instruments (Trenton)-cooled I-PentaMAX camera with MetaMorph software (Universal imaging).

23. Lenzen, C., Cool, R. H. & Wittinghofer, A. Analysis of intrinsic and CDC25-stimulated guanine nucleotide exchange of p21ras-nucleotide complexes by fluorescence measurements. *Methods Enzymol.* **255**, 95–109 (1995).
24. Van Duyne, G. D., Standaert, R. F., Karplus, P. A., Schreiber, S. L. & Clardy, J. Atomic structures of the human immunophilin FKBP-12 complexes with FK506 and rapamycin. *J. Mol. Biol.* **229**, 105–124 (1993).
25. Kabsch, W. Automatic processing of rotation diffraction data from crystals of initially unknown symmetry and cell constants. *J. Appl. Crystallogr.* **26**, 795–800 (1993).
26. Sheldrick, G. M. & Schneider, T. R. SHELXL: High-resolution refinement. *Methods Enzymol.* **277**, 319–343 (1997).
27. de la Fortelle, E. & Bricogne, G. in *Methods in Enzymology* (eds Carter, C. W. Jr & Sweet, R. M.) 472–494 (1997).
28. McRee, D. E. XtalView-Xfit—A versatile program for manipulating atomic coordinates and electron density. *J. Struct. Biol.* **125**, 156–65 (1999).
29. Murshudov, G. N., Vagin, A. A. & Dodson, E. J. Refinement of macromolecular structures by the maximum-likelihood method. *Acta Crystallogr. D* **53**, 240 (1997).
30. Laskowski, R. A., MacArthur, M. W., Moss, D. S. & Thornton, J. M. Procheck—a program to check the stereochemical quality of protein structures. *J. Appl. Crystallogr.* **26**, 283–291 (1993).
31. Kraulis, P. J. Molscript—a program to produce both detailed and schematic plots of protein structures. *J. Appl. Crystallogr.* **24**, 946–950 (1991).
32. Merritt, E. A. & Murphy, M. E. Raster3D Version 2.0. A program for photorealistic molecular graphics. *Acta Crystallogr. D* **50**, 869–73 (1994).
33. Landau, M. et al. ConSurf 2005: the projection of evolutionary conservation scores of residues on protein structures. *Nucleic Acids Res.* **33**, W299–W302 (2005).
34. Potterton, E., McNicholas, S., Krissinel, E., Cowtan, K. & Noble, M. The CCP4 molecular graphics project. *Acta Crystallogr. D* **58**, 1955–1957 (2002).
35. DeLano, W. L. *The PyMOL Molecular Graphics System* (DeLano Scientific, Palo Alto, California, USA, 2002).
36. Guex, N. & Peitsch, M. C. SWISS-MODEL and the Swiss-PdbViewer: An environment for comparative protein modeling. *Electrophor.* **18**, 2714–2723 (1997).
37. Collaborative Computational Project. The CCP4 suite: programs for protein crystallography. *Acta Crystallogr. D* **50**, 760 (1994).
38. Philo, J. S. A method for directly fitting the time derivative of sedimentation velocity data and an alternative algorithm for calculating sedimentation coefficient distribution functions. *Analyt. Biochem.* **279**, 151–163 (2000).

39. Philo, J. S. Improved methods for fitting sedimentation coefficient distributions derived by time-derivative techniques. *Analyt. Biochem.* 354, 238–246 (2006).
40. Laue, T. M., Shah, B. D., Ridgeway, T. M. & Pelletier, S. L. in *Analytical Ultracentrifugation in Biochemistry and Polymer Science* (eds Harding, S. E., Rowe, A. J. & Horton, J. C.) 90–125 (Roy. Soc. of Chem., Cambridge, UK, 1992).